Accepted version

John P. Vtkovsk, Anton Bergant, Angus R. Simpson and Martin F. Lambert
Systematic evaluation of one-dimensional unsteady friction models in simple pipelines
Journal of Hydraulic Engineering, 2006; 132(7):696-708

http://doi.org/10.1061/(ASCE)0733-9429(2006)132:7(696)

Systematic evaluation of one–dimensional unsteady friction models in simple pipelines

by

Vítkovský, J., Bergant, A., Simpson, A.R. and Lambert, M.F.

Journal of Hydraulic Engineering

Citation:
Vítkovský, J., Bergant, A., Simpson, A.R. and Lambert, M.F. (2006). "Systematic evaluation of one–dimensional unsteady friction models in simple pipelines." *Journal of Hydraulic Engineering*, American Society of Civil Engineers, Vol. 132, No. 7, July, 696-708. (29 citations to Jan. 2013 – Scopus)

SYSTEMATIC EVALUATION OF ONE-DIMENSIONAL UNSTEADY FRICTION MODELS IN SIMPLE PIPELINES

By John P. Vítkovský[1], Anton Bergant[2], Angus R. Simpson[3], M. ASCE,

and Martin F. Lambert[4]

CE DATABASE KEYWORDS

Friction; Pipes; Transients; Unsteady Flow; Numerical Analysis; Error Analysis

---

[1] Graduate Hydrologist, Water Assessment Group, Department of Natural Resources and Mines, Indooroopilly QLD 4068, Australia. Email: john.vitkovsky@nrm.gov.qld.au

[2] Head, Research, Instrumentation and Control Engineering Department, Litostroj E.I. d.o.o., 1000 Ljubljana, Slovenia. Email: anton.bergant@litostroj-ei.si

[3] Head, Associate Professor, Centre for Applied Modelling in Water Engineering, School of Civil and Environmental Engineering, University of Adelaide, Adelaide SA 5005, Australia. (Corresponding author). Tel: +61 8 8303 5874; Fax: +61 8 8303 4359; Email: asimpson@civeng.adelaide.edu.au

[4] Associate Professor, Centre for Applied Modelling in Water Engineering, School of Civil and Environmental Engineering, Univ. of Adelaide, Adelaide SA 5005, Australia. Email: mlambert@civeng.adelaide.edu.au

ABSTRACT

In this paper, basic unsteady flow types and transient event types are categorised, and then unsteady friction models are tested for each type of transient event. One important feature of any unsteady friction model is its ability to correctly model frictional dissipation in unsteady flow conditions under a wide a range of possible transient event types. This is of importance to the simulation of transients in pipe networks or pipelines with various devices in which a complex series of unsteady flow types are common. Two common one-dimensional unsteady friction models are considered, namely the constant coefficient instantaneous acceleration-based model and the convolution-based model. The modified instantaneous acceleration-based model, although an improvement, is shown to fail for certain transient event types. Additionally, numerical errors arising from the approximate implementation of the instantaneous acceleration-based model are determined, suggesting some previous good fits with experimental data are due to numerical error rather than the unsteady friction model. The convolution-based model is successful for all transient event types. Both approaches are tested against experimental data from a laboratory pipeline.

INTRODUCTION

Transient flow occurs in pipelines when the pressure and flow rate change with time. Traditionally, pipe friction during transient events has been modelled using steady friction approximations, such as the Darcy-Weisbach friction equation (shown below) or similar. As early as the 1950's researchers (Daily *et al*., 1956) realised that the steady friction approximation produced an insufficient amount of damping as compared to experimental

behavior. Unsteady friction models were introduced to account for this lack of damping. The basic governing equations for one-dimensional unsteady pipe liquid flow ($V << a$) are

$$\frac{\partial H}{\partial t} + \frac{a^2}{g}\frac{\partial V}{\partial x} = 0 \quad \text{and} \quad \frac{\partial H}{\partial x} + \frac{1}{g}\frac{\partial V}{\partial t} + J_S + J_U = 0 \tag{1}$$

where H = piezometric head (head), V = average velocity, a = wave speed, g = gravitational acceleration, x = distance, t = time and J_S and J_U are the head losses per unit length due to steady and unsteady friction respectively (Vardy, 1980). The steady component of the friction may be based on the Darcy-Weisbach friction relationship and is defined as

$$J_S = \frac{fV|V|}{2gD} \tag{2}$$

in which f = Darcy-Weisbach friction factor and D = pipe diameter. A large number of unsteady friction models have been proposed in the literature, however, most have only been experimentally validated for certain types of transient events (predominantly a full downstream valve closure). This paper focuses on a systematic categorisation of both unsteady flow types and transient event types. During the consideration of these unsteady flow and transient event types, two distinct one-dimensional unsteady friction models are considered.

The first one-dimensional unsteady friction model considered in this paper is based on the instantaneous acceleration of the fluid (Daily *et al*., 1956; Carstens and Roller, 1959; Golia, 1990; Brunone *et al*. 1991). The model that is considered in this paper is the Brunone *et al*. (1991) model and is hereafter referred to as the instantaneous acceleration-based (IAB) model.

$$J_U = \frac{k}{g}\left(\frac{\partial V}{\partial t} - a\frac{\partial V}{\partial x}\right) \tag{3}$$

where the coefficient k is either experimentally calibrated or determined numerically from another, more physically accurate, model (Pezzinga, 2000). The IAB model considered in this paper assumes a constant k coefficient. After the submission of this paper two conference papers were published that consider a k coefficient that varies with time and space (Brunone *et al*. 2003, Bouazza and Brunelle 2004). The coefficient k for these models was back calculated from more a complex unsteady model and, therefore, more complex behavior can be replicated. The results from these models show promise so long as they are sufficiently tested.

The second one-dimensional unsteady friction model considered in this paper is based on Zielke (1968) with the convolution of previous fluid accelerations and a weighting function. In this paper this type of model is referred to as the convolution-based (CB) model.

$$J_U = \frac{16\nu}{gD^2}\int_0^t \frac{\partial V}{\partial t}\left(t^*\right)W\left(t-t^*\right)dt^* \qquad (4)$$

where ν = kinematic viscosity and W = weighting function. The weighting function is determined using the "frozen viscosity" assumption based on the steady-state viscosity distribution. Zielke (1968) determined the weighting function for laminar flows. Unfortunately the computer solution of the convolution in Eq. 4 is time consuming. Trikha (1975) improved computational speed, but at the expense of solution accuracy. Kagawa *et al*. (1983) and then Suzuki *et al*. (1991) created implementations with both high accuracy and high computational efficiency. Vardy and Brown (1995) determined a set of weighting functions for the convolution-based approach for smooth-pipe turbulent flows. Recently, Ghidaoui and Mansour (2002) efficiently implemented the Vardy-Brown weighting function in the method of characteristics; however, like the Trikha (1975) implementation of Zielke's weighting function, accuracy was decreased as a trade-off for increased computational speed.

CLASSIFICATION OF SIMPLE UNSTEADY FLOW TYPES

For the purpose of testing the one-dimensional unsteady friction models, a number of unsteady flow types are formulated in this section. In one-dimensional steady flow there are two flow situations to consider based on the flow direction (if laminar and turbulent flow regimes are ignored initially). The average velocity (V) of the fluid easily describes the two flow types—positive and negative. However, in unsteady flow there are additional flow type classifications. The product of the velocity and the acceleration describes whether the fluid is accelerating or decelerating. If $V(\partial V/\partial t) > 0$ then the fluid is accelerating, if $V(\partial V/\partial t) < 0$ then the fluid is decelerating. Finally, the product of the temporal and spatial accelerations describes the direction of the wave propagation. If $(\partial V/\partial t)(\partial V/\partial x) > 0$ then the wave is propagating in the negative x direction, if $(\partial V/\partial t)(\partial V/\partial x) < 0$ in the positive x direction. Consideration of these three properties results in eight possible unsteady flow types. The eight unsteady flow types are based on:

(i) velocity in the positive and negative directions,

(ii) acceleration and deceleration and

(iii) propagation of the pressure wave in the positive and negative x directions.

Table 1 summarises the different unsteady flow types. These unsteady flow types are used later to describe the behavior of unsteady friction models.

CLASSIFICATION OF SIMPLE TRANSIENT EVENT TYPES IN A PIPELINE

The eight unsteady flow types in Table 1 only apply to monotonically accelerating or decelerating flows. Water hammer events in pipelines and pipe networks contain combinations of the unsteady flow types. It becomes useful, in a practical sense, to define

some basic set of transient events by examining a simple system comprised of a single pipeline between two reservoirs. A valve located next to each reservoir initiates the transient event. The starting conditions for the eight different types of transient event may be depicted as shown in Figure 1, in which V_0 is the initial steady-state velocity (before a transient event) for valve closure events and V_F is the final steady-state velocity (after a transient event) for valve opening events. The initial hydraulic grade lines are also shown between each tank. The systems are considered frictionless. These events are related to the eight unsteady flow types by imagining the first pressure rise or fall immediately after the valve is either closed or opened instantaneously. The initial unsteady flows of transient event types E1 to E8 correspond to unsteady flow types U1 to U8. Transient event types E1 & E6, E2 & E5, E3 & E8 and E4 & E7 are mirror images of each other with respect to the direction of flow, thus reducing the number to four distinct cases. These eight transient event types are used in a latter section to check the performance of the instantaneous acceleration-based (IAB) unsteady friction model.

Each transient event generates a sequence of unsteady flow types that repeats based on the natural frequency of the pipeline system. Consider the downstream valve closure event (type E4). Figure 2 shows the behavior of pressure and velocity for the first natural period of the pipeline system after an instantaneous valve closure at time $t = 0$. The sequence of unsteady flow types for each period (L/a, where L = pipe length) of the transient is summarised as S2, U4, U5, U3, U6, U4, … (the sequence of flow types repeats with a period of $4L/a$). Table 2 shows the unsteady flow types during each period of L/a for each transient event type.

Each transient event has a repetition of unsteady flow types that does not change. Additionally, each transient event can be paired up with another event that has the same

sequence of unsteady flow types, but starts at different positions in the sequence. The pairs of events are E1 & E5, E2 & E6, E3 & E4 and E7 & E8. Note that for experimental testing, only half of the events are required to be tested because the other half are found by reversing the co-ordinate system. The natural period of the pipeline is dependent on the boundary conditions. For those cases where the boundary conditions are a closed valve and a reservoir (events E3, E4, E7 and E8) the natural period is $4L/a$. For the other events where both boundary conditions are reservoirs (events E1, E2, E5 and E6) the natural period is $2L/a$.

For transients in a pipe network it is likely that there is no repeating sequence of unsteady flow types. Consider the example network given in Liggett and Chen (1994) and shown in Figure 3(a). A transient is generated by the instantaneous closure of a side discharge at node 6 at a time of 1.0 s. Figure 3(b) shows the unsteady flow types in pipe 7 that result from the closure of the side discharge. A complex sequence of unsteady flow states result. Additionally, for slower transients it is less likely that such a defined sequence of unsteady flow types result. The purpose of the defined unsteady events will become apparent when considering the systematic testing of unsteady friction models. An unsteady friction model must be able to perform correctly for a wide variety of flow types to accurately model pipe network transients.

SIGN DIAGRAM APPROACH FOR A MODIFIED INSTANTANEOUS ACCELERATION-BASED FORMULATION

The IAB unsteady friction model (Eq. 3) was developed to remove the need for the Heaviside operator used by Golia (1990) yet still producing similar results. The concept behind the Golia model was that the model should produce damping in accelerating flows only (see

correct J_U sign column in Table 3). Considering the IAB model, a sign table is created based on the sign of J_U for each unsteady flow type (see J_U component signs and total sign in Table 3). In half of the cases (U1, U2, U7 and U8) the model returns the correct signs of J_U. The cases that show incorrect signs have either no cancellation where there should be some (U3 and U4) or cancellation where there should be none (U5 and U6).

For events E3 and E4 the IAB model produces amplification rather than damping. This amplification occurs because events E3 and E4 contain the unsteady flow conditions U3, U4, U5 and U6 (see Table 2) of which U3 and U4 produce amplification when using the IAB unsteady friction model (see Table 3, total J_U has an incorrect sign compared to the Golia J_U). Alternatively, transient events E7 and E8 produce damping because they contain unsteady flow types U1, U2, U7 and U8 (see Table 3, total J_U has a correct sign compared to the Golia J_U). Figure 4 shows the head response at the valve for transient event types E3 and E7 where the sign diagram of the IAB model predicts there should be amplification and damping respectively. The method of characteristics staggered grid is used for all computational cases in the paper.

For steady friction, the head loss for a steady flow is proportional to the square of the velocity for the Darcy-Weisbach formulation. However, for a generalised flow case where the flow might be positive or negative the following modification was made

$$\frac{dH}{dx} = -\frac{fV^2}{2gD} \quad \text{changed to} \quad \frac{dH}{dx} = -\frac{fV|V|}{2gD} \tag{5}$$

Similarly, to address the problem of amplification, the sign of the convective term in the IAB model may be modified (independently formulated by Bergant *et al*., 1999; Pezzinga, 2000; Bergant *et al*. 2001). This modification—termed the modified instantaneous acceleration-based (MIAB) model—ensures that the unsteady friction magnitude is negligible during

deceleration and substantial during acceleration. Also when the fluid is accelerating, the sign of the unsteady friction term is such that the shear stress acts in the opposite direction to the flow (thus damping occurs). These modifications lead to

$$J_U = \frac{k}{g}\left(\frac{\partial V}{\partial t} + a\phi_A \frac{\partial V}{\partial x}\right) \tag{6}$$

where the convective acceleration term has been multiplied by an operator ϕ_A that depends on the sign of the convective acceleration. The operator is defined as ϕ_A = {+1 if $V \times \partial V/\partial x \geq 0$; or −1 if $V \times \partial V/\partial x < 0$}. Table 4 shows that the modified formulation produces the correct sign of J_U (as compared to Golia, 1990) in all eight unsteady flow types. Figure 4 shows the behavior of the MIAB model for transient event types E3 and E7. Now damping is observed for both events; however, the following section presents results for other transient event types where unrealistic behavior is still observed even if the MIAB model (Eq. 6) is used.

DAMPING IN THE MODIFIED INSTANTANEOUS ACCELERATION-BASED MODEL

This section shows that it is only the convective acceleration term in the IAB and MIAB models that is the cause of damping. Consider the effect of the unsteady friction alone (ignoring the steady friction component in Eq. 1). The equations of continuity and motion may be re-written with the MIAB model inside the square brackets as

$$\frac{\partial H}{\partial t} + \frac{a^2}{g}\frac{\partial V}{\partial x} = 0 \quad \text{and} \quad \frac{\partial H}{\partial x} + \frac{1}{g}\frac{\partial V}{\partial t} + \left[\frac{k}{g}\frac{\partial V}{\partial t} + \frac{ak\phi_A}{g}\frac{\partial V}{\partial x}\right] = 0 \tag{7}$$

Now consider the following substitutions in Eq. 7

$$g' = \frac{g}{(1+k)}, \quad a' = \frac{a}{\sqrt{1+k}} \quad \text{and} \quad k' = \frac{k}{\sqrt{1+k}} \tag{8}$$

Thus

$$\frac{\partial H}{\partial t}+\frac{(a')^2}{g'}\frac{\partial V}{\partial x}=0 \quad \text{and} \quad \frac{\partial H}{\partial x}+\frac{1}{g'}\frac{\partial V}{\partial t}+\left[\frac{a'k'\phi_A}{g'}\frac{\partial V}{\partial x}\right]=0 \tag{9}$$

Since the first two terms of both equations are the wave equation, which is non-dissipative, the damping due to the unsteady friction model must come solely from the $\partial V/\partial x$ term from the IAB model in Eq. 9 (in square brackets). The $\partial V/\partial t$ term in Eq. 6 from the IAB model only contributes to a modification in g and a and does not add to the damping. Considering the modification made to the IAB model in the previous section (using the sign operator ϕ_A), it is therefore not surprising that the modification is applied only to the convective acceleration term that causes the damping. Eq. 9 also shows that the acceleration-based models also affect the Joukowsky pressure rise relationship and the natural frequency of the pipeline system through modification of the wave speed and gravitational acceleration.

Considering the form of Eq. 9, the MIAB model can be split into two parts. The temporal acceleration part does not produce any damping but rather only a wave speed change that doesn't affect damping (an inertial portion). The convective acceleration part produces only damping (a dissipation portion). This introduces two unsteady friction coefficients that require calibration (k_A and k_P) either to experimental data or numerical data that includes a higher-order physically-based unsteady friction model. Potentially, since the coefficients k_A and k_P have different behavior, they could be determined separately—k_A from the extra damping and k_P from the change in the effective wave speed.

$$J_U=\frac{k_P}{g}\frac{\partial V}{\partial t}+\frac{a\phi_A k_A}{g}\frac{\partial V}{\partial x} \tag{10}$$

The two unsteady friction coefficients may be used to control the influence of additional inertial and frictional forces. During the revision stage of this paper two conference papers were published that take a similar approach to Eq. 10 (Loureiro and Ramos 2003, Abreu and Almeida 2004). The k_P coefficient can be linked to the momentum correction factor, β, by

$k_P \approx \beta - 1$ for low frequency disturbances (Brown *et al.*, 1969). The coefficient k_A may be interpreted as the extra frictional damping due to the unsteady shear stress. Vítkovský (2001) roughly estimated $k_A \approx 0.166\sqrt{f}$, but with minimal experimental validation only. Both k_A and k_P are kept constant for the modelling of short duration unsteady events, although, in general are likely to be both frequency-dependent and time-dependent. Although this model still has the same shortcomings as the MIAB model, the model does however offer considerable flexibility for calibrating to unsteady friction events.

PROBLEMS WITH THE MODIFIED INSTANTANEOUS ACCELERATION-BASED MODEL FOR VALVE-OPENING EVENTS

In the closure to the paper Axworthy *et al*. (2000), the authors presented a characteristic solution for the unsteady pipe flow equations including the MIAB unsteady friction model. The compatibility equations for the positive and negative characteristics are respectively

$$dH + \frac{(1+k)}{\left[1+\frac{1}{2}k(1-\phi_A)\right]}\frac{a}{g}dV + \frac{fV|V|}{2gD}dx = 0 \quad \text{along} \quad \frac{dx}{dt} = \frac{a}{1+\frac{1}{2}k(1-\phi_A)} \tag{11}$$

$$dH - \frac{(1+k)}{\left[1+\frac{1}{2}k(1+\phi_A)\right]}\frac{a}{g}dV - \frac{fV|V|}{2gD}dx = 0 \quad \text{along} \quad \frac{dx}{dt} = -\frac{a}{1+\frac{1}{2}k(1+\phi_A)} \tag{12}$$

The method of characteristics solution shows that the slope of characteristic lines is dependent on the instantaneous flow conditions (dx/dt is a function of ϕ_A, which is dependent on the instantaneous velocity and convective acceleration). Figure 5 demonstrates the variable slope characteristics in the characteristic grid.

Consider the case of a tank-valve-pipeline-tank system in which the valve is initially closed and the pressure in the right-hand tank is greater than the pressure in the left-hand tank

(shown in Figure 6(a)). The rapid opening of the valve creates a transient such that the flow only accelerates and never decelerates. Figure 6(b) shows a characteristic diagram for the valve-opening case (transient event type E2). In this analysis steady friction is ignored ($f = 0$) therefore the compatibility equations represent an exact solution of the unsteady pipe flow equations including unsteady friction.

The propagation of the disturbance generated from the sudden opening of the valve is tracked. First the wave travels from point A to B in Figure 6(b) along a positive characteristic. The fluid accelerates from a velocity of zero as the wave travels along the pipe. In this case, the convective acceleration is positive ($\partial V/\partial x > 0$) and the velocity is negative ($V < 0$), therefore ϕ_A is negative (−1). The compatibility equation (Eq. 11) for the positive characteristic becomes

$$dH + \frac{a}{g} dV = 0 \quad \text{along} \quad \frac{dx}{dt} = \frac{a}{1+k} \tag{13}$$

Once the disturbance reaches B, it reflects off tank 2 with an additional acceleration of the fluid. Then the wave travels from point B to C along a negative characteristic. In this case, the convective acceleration is negative ($\partial V/\partial x < 0$) and the velocity is negative ($V < 0$), therefore ϕ_A is positive (+1). The compatibility equation for the negative characteristic (Eq. 12) becomes

$$dH - \frac{a}{g} dV = 0 \quad \text{along} \quad \frac{dx}{dt} = -\frac{a}{1+k} \tag{14}$$

This process repeats until the final steady state condition is attained. Considering the form of Eqs. 13 and 14—that are an exact solution—the unsteady friction model does not affect the magnitude of the transient waves, thus no damping of the waveform occurs. Also, the effective wave speed of the transient waves is decreased by a factor of $(1+k)$. The lack of extra damping for this event-type shows a failure of the MIAB unsteady friction model.

Figure 7 shows a numerical simulation using both the IAB and MIAB models depicting this behavior. As expected, there is no damping, just a change in the effective wave speed. A similar result from the simulation of valve-closure events (Figure 4) shows a lack of shape-change of the transient, which is a result of frequency-independent damping. Ghidaoui *et al*. (2001) stated the reason for this is that the damping from the MIAB model only occurs from interaction with the boundary, rather than along the pipe.

This section has shown that, although the modification to the IAB model corrected behavior in some transient events, the model still produces unrealistic behavior for other transient events (valve opening events).

NUMERICAL ATTENUATION AND DISPERSION IN THE INSTANTANEOUS ACCELERATION-BASED MODEL

The MIAB unsteady friction model has previously shown good matches with experimental tests based on downstream and upstream valve closures. The damping and smoothing exhibited by the experimental data is well produced by the MIAB model; however, the numerical solution of the transient equations including the unsteady friction model was performed for limited number of transient event types and numerical parameters. The exact MOC solution of the IAB model was tested by Bughazem and Anderson (1996, 2000), Wylie (1997) and Vítkovský (2001); however, interpolation was required to apply the exact method of characteristics (MOC) compatibility equations to a fixed grid (an approximation). An approximate MOC solution of the IAB model that uses a finite difference approximation of the derivatives in the unsteady friction model was investigated by Brunone *et al*. (1991), Bergant and Simpson (1994), Bughazem and Anderson (1996) and Bergant *et al*. (1999,

2001). Approximation in the application of unsteady friction adds some numerical attenuation and dispersion, thus masking the true performance of the unsteady friction model. As an example of a source of numerical error, consider the positive and negative characteristics for the IAB model as defined in Figure 8 on a fixed MOC grid. The Courant number, C_r, for the positive characteristic is $C_r = 1$, whereas for the negative characteristic $C_r = 1/(1+k)$. When the Courant number differs from unity numerical error is present. Interpolation schemes can minimise the numerical error, but not eliminate it. A similar argument may be formed for the MIAB model, however, in this case, the Courant number for the positive and negative characteristics depend on ϕ_A, which in turn depends on the local flow conditions (see Figure 5), and varies between $C_r = 1$ and $C_r = 1/(1+k)$. Historically, the prediction and quantification of numerical error in the simulation of pipeline transients can be subdivided into three main areas: (1) errors due to the interpolation scheme in the MOC, (2) errors from different finite-difference schemes, and (3) errors due to the steady friction implementation. Wiggert and Sundquist (1977) used the Fourier method to calculate the frequency-dependent attenuation and dispersion numerical error for a linear space-line interpolation scheme in the MOC. Similarly, Goldberg and Wylie (1983) used the Fourier method to investigate the attenuation and dispersion coefficients for the reach-out and reach-back linear time-line interpolation schemes. However, the Fourier method is only one approach that can be used to quantify numerical error. Some other approaches have used dimensionless parameters to describe the numerical error associated with spline and Hermite interpolations (Sibetheros *et al*., 1985), equivalent hyperbolic differential equations (EHDE) to investigate the error from numerical MOC interpolation schemes (Ghidaoui and Karney, 1994), and total error norms to describe the error resulting from numerical calculation of transients using the MacCormack, Lambda and Gabutti Schemes (Chaudhry and Hussaini, 1985). The previously mentioned analyses neglected friction when assessing numerical error.

Maudsley (1984) used an approach similar to the Fourier method to check the numerical errors from a finite difference scheme including friction. This approach was used by Wylie (1983), Holloway and Chaudhry (1985) and Anderson *et al*. (1991) for investigation of both the stability and accuracy of the MOC solution for transient pipe flow when steady friction was included. Wylie (1996) investigated the error due to the inclusion of steady friction based on dimensionless numbers that describe steady friction.

In this paper, a study of the numerical error associated with the application of an unsteady friction model is performed using the Fourier method. The Fourier method assumes that the head and velocity associated with a disturbance in the MOC grid can be described by the summation

$$\nu(x,t) = \sum_{j=1}^{\infty} \nu_j e^{i(\sigma_j x + \beta_j t)} \tag{15}$$

where ν represents either H or V and ν_j, σ_j and β_j are constants for the j^{th} harmonic component. The dependent variables ν at the grid points are substituted into the numerical scheme and rearranged for $\nu(x, t)$. This results in an expression that can be written in the form $[A]\{\nu(x, t)\}=\{0\}$, where $[A]$ is a 2×2 coefficient matrix. The solution involves the calculation of eigenvalues found by setting the determinant of $[A]$ to zero to avoid the trivial solution. Analysis using the imaginary part of β_j shows the attenuation of the numerical scheme in time. A similar analysis using the real part of β_j shows the dispersion of the numerical scheme (Wiggert and Sundquist, 1977). The Fourier method produces two coefficients R_1 and R_2 that describe the attenuation and dispersion, respectively, of the numerical scheme for different frequency disturbances. The R_1 coefficient represents the exponential attenuation ($R_1 < 1$) error of certain frequency disturbances by the numerical scheme. The R_2 coefficient

is a ratio of the numerical wave speed of a certain frequency disturbance to the true wave speed and represents the dispersion error.

For the analysis of numerical error of the MIAB model, problems arise due to ϕ_A being different for each characteristic and for different flow types. To simplify the analysis the IAB model is used for the study of numerical error. The Fourier method is applied first to the exact MOC solution of the IAB model and then to an approximate MOC solution of the IAB model that uses a finite difference to incorporate the derivatives. The exact solution to IAB model was performed by Bughazem and Anderson (1996) and then by Wylie (1997). The resulting compatibility equations were

$$dH + \frac{a}{g}dV + \frac{fV|V|}{2gD}dx = 0 \quad \text{along} \quad \frac{dx}{dt} = \frac{a}{1+k} \tag{16}$$

$$dH - \frac{a(1+k)}{g}dV - \frac{fV|V|}{2gD}dx = 0 \quad \text{along} \quad \frac{dx}{dt} = -a \tag{17}$$

Figure 8 shows a representation of the MOC solution at a point P using the compatibility equations.

Applying the Fourier method to Eqs. 16 and 17, the attenuation and dispersion coefficients for the exact solution of the IAB model ignoring the steady state friction term are

$$R_1 = 1 \quad \text{and} \quad R_2 = \frac{1}{1+k} \tag{18}$$

The Fourier method predicts no attenuation by the unsteady friction model, only a decrease in the effective wave speed by a factor of $(1 + k)$. This implies that, in the absence of boundary conditions, the IAB model will not produce any damping or any smoothing of the pressure oscillations. For the exact solution of the IAB model both R_1 and R_2 are frequency independent.

Now consider the MOC compatibility equations including the IAB model, again ignoring the steady friction. Here, the IAB model has not been included in the standard MOC solution for unsteady pipe flow, but incorporated as a finite difference approximation.

$$dH \pm \frac{a}{g} dV \pm \frac{k}{g}\left[\left(\frac{\partial V}{\partial t}\right)^{\pm} - a\left(\frac{\partial V}{\partial x}\right)^{\pm}\right]dx = 0 \quad \text{along} \quad \frac{dx}{dt} = \pm a \tag{19}$$

The partial derivatives in the unsteady friction term are approximated by finite-difference approximations on the characteristic grid. The finite differences are represented on the characteristic grid in Figure 9. They were chosen such that they do not encroach on adjacent computational sections and are therefore untroubled by proximity to boundary conditions or pipe junctions. Written mathematically, the finite differences considered for each characteristic are

C^+: $$\left(\frac{\partial V}{\partial t}\right)^{+} \approx \frac{V(A) - V(A_0)}{\Delta t} \quad \text{and} \quad \left(\frac{\partial V}{\partial x}\right)^{+} \approx \frac{V(P_0) - V(A)}{\Delta x} \tag{20}$$

C^-: $$\left(\frac{\partial V}{\partial t}\right)^{-} \approx \frac{V(B) - V(B_0)}{\Delta t} \quad \text{and} \quad \left(\frac{\partial V}{\partial x}\right)^{-} \approx \frac{V(B) - V(P_0)}{\Delta x} \tag{21}$$

Applying the Fourier method to the compatibility equations containing the finite difference approximation of the unsteady friction derivatives yields the numerical error measures R_1 and R_2. The dimensionless disturbance period is $T_j/\Delta x$, where T_j is the period of the disturbance in the x-direction and Δx is the grid spacing. Figure 10 shows the variation of R_1 and R_2 with the frequency of disturbance for different unsteady friction coefficient (k) values.

The results show that both the attenuation and dispersion coefficients are frequency-dependent. For high frequency disturbances (low values of $T_j/\Delta x$), a great deal of numerical attenuation occurs, whereas for low frequency disturbances little or no numerical attenuation

occurs. The dispersion coefficient is equal to unity for the highest frequency disturbances (the highest where one full period fit exactly into two grid steps, $T_j/\Delta x = 2$) because the highest possible frequency disturbance is limited by the grid spacing and thus must travel at the wave speed ($a = \Delta x/\Delta t$). However, as the dimensionless period of the disturbance increases, the dispersion coefficient decreases and approaches $1/(1 + k)$, which is equal to the dispersion coefficient for the exact solution of the IAB model (see Eq. 18).

Figure 11 shows the behavior of R_1 and R_2 as a function of the unsteady friction coefficient. As expected, as k approaches zero both R_1 and R_2 approach unity. As k increases, both R_1 and R_2 decrease meaning greater attenuation and dispersion of the numerical solution. The exception is for R_2 when $T_j/\Delta x$ equals two and the propagation of information is limited to the spacing of the grid (full period of the disturbance just fits in $2\Delta x$). For that case no dispersion occurs ($R_2 = 1$).

There are a number of limitations associated with the Fourier method of analysis. One problem is that boundary conditions are not considered and the initial conditions are assumed periodic. Also, particular to the MIAB model, the Fourier method does not consider the different unsteady flow types that influence ϕ_A.

The numerical error behavior, shown in Figure 10 and Figure 11, for the IAB model is tested numerically using the MOC and the MIAB model. Figure 12 shows the pressure response at the quarter point of a pipeline (H_Q) for a valve-opening event (transient event type E1) with different grid discretisations (defined by the number of reaches the pipeline has been divided). Two cases are considered; the first uses 16 reaches and the second 4096 reaches. The small discretisation case of 16 reaches shows considerable numerical attenuation and dispersion

error, while the large discretisation case shows less error. The results clearly show the numerical attenuation and dispersion caused by approximate application of the MIAB unsteady friction model. A similar behavior is found for numerical simulations using the MIAB model and for different transient event types.

The accurate MOC analysis that includes the IAB model for valve-opening events (large discretisation case of 4096 reaches) shows no smoothing of the pressure response, suggesting that the smoothing when the unsteady friction model was treated as an addition to the steady friction is numerical in nature (numerical diffusion). This numerical smoothing behavior confirms the numerical error predicted by the Fourier method analysis. Experimental verification results performed by Brunone *et al*. (1991), Bergant and Simpson (1994) and Adamkowski and Lewandowski (2004) indicates smoothing and produces better experimental matches. On this basis one can argue that numerical diffusion is advantageous in the absence of better unsteady friction models; however, if a numerical scheme in some unintended way mimics a natural diffusive process, then this suggests that some natural diffusive component could be missing from the basic governing unsteady equations. Ultimately, one should aim to eliminate all sources of error, especially those that are numerical in nature.

The presence of numerical damping and attenuation might also account for the wide range of IAB model coefficients produced in the literature (k = 0.03 to 0.085). However, recently a degree of coincidence has been reached on k from downstream and upstream valve closure experiments. These experimentally calibrated values range from 0.028 to 0.038 for initial flows with Reynolds numbers of 2,400 to 14,400 (Wylie, 1997; Axworthy *et al*., 2000; Vítkovský, 2001). In general values of k decrease as the Reynolds number increases. These tests were for turbulent flows in hydraulically smooth pipes.

LABORATORY EXPERIMENTS

This section presents a number of experimental tests that span all transient event types considered previously in this paper. A flexible laboratory apparatus for investigating water hammer and column separation events in pipelines has been designed and constructed (Bergant and Simpson, 1995). The apparatus comprises a straight 37.2 m long sloping copper pipe of 22.1 mm internal diameter and 1.63 mm wall thickness connecting two pressurised tanks (Figure 13). The estimated relative roughness of the copper pipe walls is 0.0001. The wave speed was experimentally determined as 1,319 m/s.

Five pressure transducers are located at equidistant points along the pipeline including as close as possible to the end points. Pressures measured at the valve (H_V), quarter-point (H_Q) and at the mid-point (H_M) are considered in this paper. The water temperature in Tank 1 is continuously monitored and the valve position during closure is measured using either a potentiometer or optical sensors that are attached to the valve handle. The valve position is also recorded in the data acquisition process. Bergant and Simpson (1995) described the uncertainties in both measurement and system properties. A specified pressure in each of the tanks is controlled by a computerised pressure control system. A water hammer event in the apparatus is initiated by the rapid closure or opening of the ball valve. The initial or final steady state velocity of the flow was measured using the volume change in Tank 1 and converted to a pipe flow.

Four transient event types are tested since the remaining four are mirror-reflections of these four. The transient events correspond to event types E1, E2, E3 and E4. Tests E1 and E2 are

upstream and downstream valve openings, respectively (see Figure 1). The final steady state velocities were 1.36 m/s and 1.35 m/s corresponding to Reynolds numbers of 29,840 and 29,650. The valve opening times were 0.115 s and 0.072 s respectively. Tests E3 and E4 are upstream and downstream valve closures, respectively. Both tests have an initial velocity of 0.3 m/s corresponding to a Reynolds number of 6,584 and share a closure time of 0.009s. All tests were conducted at a temperature of 20°C. Figure 14 shows the experimental data for each test with numerical results using the quasi-steady friction model and the instantaneous acceleration-based (MIAB) unsteady friction model incorporated as finite differences. The number of reaches used was N_r = 4096 (to minimise numerical error). In addition, the unsteady friction coefficient was calibrated using experimental data from the valve closure cases resulting in k = 0.03 being adopted for all simulations.

The results in Figure 14 show a lack of damping by the MIAB model for both valve-opening events (types E1 and E2). In contrast, for the valve closure events, the MIAB model does exhibit extra damping, but does not provide any additional smoothing of the pressure oscillations (i.e., frequency independent damping). The lack of damping for transient event types E1 and E2 confirms the numerical predictions made earlier in this paper that the MIAB model does not produce any damping for valve-opening events. Figure 15 shows the results for the convolution-based (CB) unsteady friction model. The Zielke (1968) weighting function was used for transient event types E1 and E2 where the initial flow is laminar (or zero), while the Vardy and Brown (1995) weighting function was used for transient event types E3 and E4 where the initial flow is turbulent. A standard approximate MOC solution of the CB unsteady friction model that incorporates the unsteady friction term into a finite difference scheme was used. The CB unsteady friction model produces the correct behavior

for each unsteady flow event type and better reproduces the changing shape pressure oscillation with time.

It should be noted that the steady friction, the MIAB and CB models all predict the initial couple of oscillations in the transient well. The ability to correctly model the longer-term behavior of transients is only required for certain applications, such as inverse transient analysis (Liggett and Chen 1994).

CONCLUSIONS

A systematic approach for the characterisation of transient flow types and transient event types provides a basis for testing of unsteady friction models. Eight unsteady flow types and eight basic transient event types have been identified. A standard set of transient events is identified in this paper that all unsteady friction models should be able to successfully simulate. The ability to simulate a wide variety of unsteady flow types is vital when modelling pipe networks, where many types of unsteady flow conditions occur.

The constant coefficient instantaneous acceleration-based (IAB) model has been shown deficient for certain types of transient events, such as an upstream valve closure (e.g., event type E3). Using a sign diagram approach, these failure events were identified and a modified instantaneous acceleration-based (MIAB) model proposed. However, even after modification, the MIAB model failed to correctly model some types of transient events, such as valve-opening events (E1, E2, E5 and E6). This shows a general deficiency in the model. Additionally, both the IAB and MIAB models do not produce a frequency-dependent frictional behavior, as produced by more complex numerical models and observed in

experimental testing. Analysis using the Fourier method showed numerical attenuation and dispersion of the IAB model when approximately implemented in the MOC as finite differences. The presence of numerical attenuation and dispersion has been shown to be a possible cause of some previously reported good matches with experimental data and variability in the calibrated unsteady friction coefficient (k). It should be stated, though, that the analysis presented in the paper considers the behavior of the unsteady friction model alone. It is possible that the unsteady and the steady friction models may interact and their combined dissipation might be slightly larger than the sum of their individual dissipation, although this is suspected to be a second-order effect.

Experimental data have been presented for a basic set of transient events. The MIAB model showed poor matches with valve-opening tests and adequate matches with valve-closure tests, although the change in the shape of the transient response was not correctly predicted. In contrast with the MIAB model, the convolution-based (CB) models correctly simulate all transient event types. That said, the IAB and MIAB models can be used to adequately simulate transient flow for certain transient event types (IAB for events E7 and E8; MIAB for events E3, E4, E7 and E8). Additionally, since the IAB and MIAB models produce frequency-independent behavior, their application should be limited to transients with a small range of frequency components, e.g. slower transient events. These conditions should be extended to other IAB models with constant coefficients.

ACKNOWLEDGEMENTS

The writers would like to acknowledge financial support from the Australian Research Council and a scholarship provided by the Australian Government for the first author, both of which assistance are gratefully appreciated.

APPENDIX I. REFERENCES

Abreu, J.M., and Almeida, A.B. (2004). "Wall Shear Stress and Flow Behaviour Under Transient Flow in a Pipe." *9th International Conference on Pressure Surges*, BHR Group, 24-26 March Ltd, Chester, UK, 457-476.

Adamkowski, A., and Lewandowski, M. (2004). "Experimental Examination of Unsteady Friction Models for Transients Pipe Flow Simulation." *9th International Conference on Pressure Surges*, BHR Group, 24-26 March, Chester, UK, 421-437.

Anderson, A., Arfaie, M., Sandoval-Pena, R., and Suwan, K. (1991). "Pipe-Friction in Waterhammer Computation." *Proceedings of the XXIV IAHR Congress*, Madrid, Spain, 2, 23-30.

Axworthy, D.H., Ghidaoui, M.S., and McInnis, D.A. (2000). "Extended Thermodynamics Derivation of Energy Dissipation in Unsteady Pipe Flow." *Journal of Hydraulic Engineering*, ASCE, 126(4), April, 276-287.

Bergant, A., and Simpson, A.R. (1994). "Estimating Unsteady Friction in Transient Cavitating Pipe Flow." *2nd International Conference on Water Pipeline Systems*, Edinburgh, Scotland, May, 3-16.

Bergant, A. and Simpson, A.R. (1995). *Water Hammer and Column Separation Measurements in an Experimental Apparatus*. Report No. R128, Dept. of Civil and Environmental Engineering, The University of Adelaide, Adelaide, Australia.

Bergant, A., Simpson, A.R., and Vítkovský, J.P. (1999). "Review of Unsteady Friction Models in Transient Pipe Flow." *9th International Meeting of the Work Group on the Behaviour of Hydraulic Machinery under Steady Oscillatory Conditions*, IAHR, 7–9 September, Brno, Czech Republic.

Bergant, A., Simpson, A.R., and Vítkovský, J.P. (2001). "Developments in Unsteady Pipe Flow Friction Modelling." *Journal of Hydraulic Research*, IAHR, 39(3), 249-257.

Bouazza, Z., and Brunelle, P.E. (2004). "A New Friction Model for Transient Pipe Flows: Development of the Frequency Dependence Approach of Brunone." *9th International Conference on Pressure Surges*, BHR Group, 24-26 March, Chester, UK, 391-404.

Brown, F.T., Margolis, D.L., and Shah, R.P. (1969). "Small-Amplitude Frequency Behavior of Fluid Lines with Turbulent Flow." *Journal of Basic Engineering*, Transactions of the ASME, Series D, 91(4), December, 678-693.

Brunone, B., Golia, U.M., and Greco, M. (1991). "Some Remarks on the Momentum Equations for Fast Transients." *Hydraulic Transients with Column Separation (9th and Last Round Table of the IAHR Group)*, IAHR, Valencia, Spain, 4-6 September, 201-209.

Brunone, B., Cacciamani, M., Calabresi, F., and Ferrante, M. (2003). "An Investigation on Unsteady-State Friction in Laminar Flow." *Pumps, Electromechanical Devices and Systems Applied to Urban Water Management*, 22-25 April, Valencia, Spain. [CDROM]

Bughazem, M.B., and Anderson, A. (1996). "Problems with Simple Models for Damping in Unsteady Flow." *7th International Conference on Pressure Surges and Transients in Pipelines and Open Channels*, BHR Group, 16-18 April, Harrogate, UK, 537-457.

Bughazem, M.B., and Anderson, A. (2000). "Investigation of an Unsteady Friction Model for Waterhammer and Column Separation." *8th International Conference on Pressure Surges*, BHR Group, The Hague, The Netherlands, 12-14 April, 483-498.

Carstens, M.R., and Roller, J.E. (1959). "Boundary-Shear Stress in Unsteady Turbulent Pipe Flow." *Journal of the Hydraulics Division*, ASCE, 95(HY2), 67-81.

Chaudhry, M.H., and Hussaini, M.Y. (1985). "Second-Order Accurate Explicit Finite-Difference Schemes for Waterhammer Analysis." *Journal of Fluids Engineering*, ASME, December, Vol. 107, 523-529.

Daily, J.W., Hankey, W.L., Olive, R.W., and Jordaan, J.M. (1956). "Resistance Coefficients for Accelerated and Decelerated Flows Through Smooth Tubes and Orifices." *Transactions of the ASME*, Vol. 78, 1071-1077.

Ghidaoui, M.S., and Karney, B.W. (1994). "Equivalent Differential Equations in Fixed-Grid Characteristics Method." *Journal of Hydraulic Engineering*, ASCE, October, 120(10), 1159-1175.

Ghidaoui, M.S., Axworthy, D.H., Zhao, M., and McInnis, D.A. (2001). "Closure to Extended Thermodynamics Derivation of Energy Dissipation in Unsteady Pipe Flow." Journal of Hydraulic Engineering, ASCE, 127(10), October, 888-890.

Ghidaoui, M.S., and Mansour, S. (2002). "Efficient Treatment of Vardy-Brown Unsteady Shear in Pipe Transients." *Journal of Hydraulic Engineering*, ASCE, 128(1), January, 102-112.

Goldberg, D.E., and Wylie, E.B. (1983). "Characteristics Method Using Time-Line Interpolations." *Journal of Hydraulic Engineering*, ASCE, May, 109(5), 670-683.

Golia, U.M. (1990). *Sulla valutazione delle forze resistenti nel colpo d'ariete*. Report No. 639 of the Department of Hydraulics, University of Napoli, Italy.

Holloway, M.B., and Chaudhry, M.H. (1985). "Stability and Accuracy of Waterhammer Analysis." *Advanced Water Resources*, September, Vol. 8, 121-128.

Kagawa, T., Lee, I., Kitagawa, A., and Takenaka, T. (1983). "High Speed and Accurate Computing Method of Frequency-Dependent Friction in Laminar Pipe Flow for Characteristic Method." *Transactions of the Japanese Society of Mechanical Engineers*, 49(447), 2638-2644.

Liggett, J.A., and Chen, L.-C. (1994). "Inverse Transient Analysis in Pipe Networks." *Journal of Hydraulic Engineering*, ASCE, 120(8), August, 934-955.

Loureiro, D., and Ramos, H. (2003). "A Modified Formulation for Estimating the Dissipative Effect of 1-D Transient Pipe Flow." *Pumps, Electromechanical Devices and Systems Applied to Urban Water Management*, 22-25 April, Valencia, Spain. [CDROM]

Maudsley, D. (1984). "Errors in the Simulation of Pressure Transients in a Hydraulic System." *Transactions of the Institute of Measurement and Control*, 6(1), Jan-Mar, 7 - 12.

Pezzinga, G. (2000). "Evaluation of Unsteady Flow Resistances by Quasi-2D or 1-D Models." *Journal of Hydraulic Engineering*, ASCE, 126(10), 778-785.

Sibetheros, I.A., Holley, E.R., and Branski, J.M. (1991). "Spline Interpolations for Water Hammer Analysis." *Journal of Hydraulic Engineering*, ASCE, October, 117(10), 1332-1351.

Suzuki, K., Taketomi, T., and Sato, S. (1991). "Improving Zielke's Method of Simulating Frequency-Dependent Friction in Laminar Liquid Pipe Flow." *Journal of Fluids Engineering*, ASME, 113, 569-573.

Trikha, A.K. (1975). "An Efficient Method for Simulating Frequency-Dependent Friction in Transient Liquid Flow." *Journal of Fluids Engineering*, ASME, 97, 97-105.

Vardy, A.E. (1980). "Unsteady Flows: Fact and Friction." *Proceedings of the 3rd International Conference on Pressure Surges*, BHRA, Canterbury, England, 15 - 26.

Vardy, A.E., and Brown, J.M.B. (1995). "Transient, Turbulent, Smooth Pipe Friction." *Journal of Hydraulic Research*, IAHR, 33(4), 435-456.

Vítkovský, J.P. (2001). *Inverse Analysis and Modelling of Unsteady pipe Flow: Theory, Applications and Experimental Verification*. PhD Thesis, March, Department of Civil and Environmental Engineering, University of Adelaide, Australia.

Wiggert, D.C., and Sundquist, M.J. (1977). "Fixed-Grid Characteristics for Pipeline Transients." *Journal of the Hydraulics Division*, ASCE, December, 103(HY12), 1403-1416.

Wylie, E.B. (1983). "Advances in the use of MOC in Unsteady Pipeline Flow." *Proceedings of the 4th International Conference on Pressure Surges*, BHRA, Bath, England, Part 2, (70), 27-37.

Wylie, E.B. (1996). "Unsteady Internal Flows - Dimensionless Numbers & Time Constants." *7th International Conference on Pressure Surges and Transients in Pipelines and Open Channels*, BHR Group, Harrogate, UK, 16-18 April, 283-288.

Wylie, E.B. (1997). "Frictional Effects in Unsteady Turbulent Pipe Flows." *Applied Mechanics Review*, ASME, 50(11), Part 2, November, 241-244.

Zielke, W. (1968). "Frequency-dependent friction in transient pipe flow." *Journal of Basic Engineering*, ASME, 90(1), 109-115.

APPENDIX II. NOTATION

A = pipe area;

a = wave speed;

C_r = Courant number;

D = pipe diameter;

f = Darcy-Weisbach friction factor;

g = gravitational acceleration;

H = piezometric head (head);

H_M, H_Q, H_V = head at mid-point, at quarter-point and at valve;

J_S = steady friction loss per unit length;

J_U = unsteady friction loss per unit length;

k = unsteady friction coefficient of the IAB and MIAB models;

k_A = unsteady friction coefficient based on unsteady friction;

k_P = unsteady friction coefficient based on fluid inertia;

L = pipe length;

N_r = number of computational reaches;

R_1 = attenuation coefficient from Fourier method;

R_2 = dispersion coefficient from Fourier method;

t, t^* = time;

T_j = period of disturbance in the spatial plane for Fourier method;

v = velocity;

V = average velocity (defined as $AV = \int_A v dA$);

W = weighting function;

x = distance;

β = momentum correction factor (defined as $\beta AV^2 = \int_A v^2 dA$);

β_j, ν_j, σ_j = Fourier method constants;

Δt = temporal grid size;

Δx = spatial grid size;

ν = kinematic viscosity;

ϕ_A = acceleration sign operator;

subscripts

F = based on final steady flow;

j = j^{th} harmonic component for Fourier method;

M = mid-point;

Q = quarter-point;

V = valve;

0 = based on initial steady flow;

superscripts

$'$ = modified variable.

LIST OF FIGURES

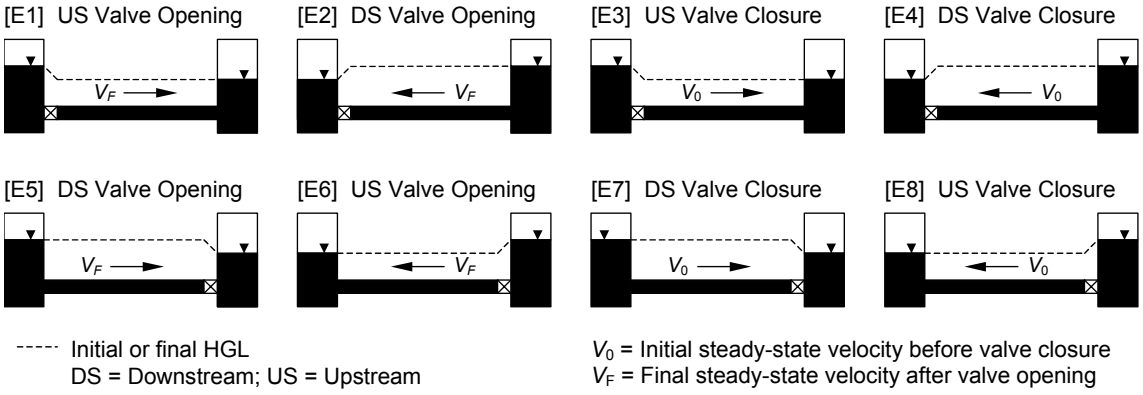

Figure 1. Initial or final conditions for eight transient event types

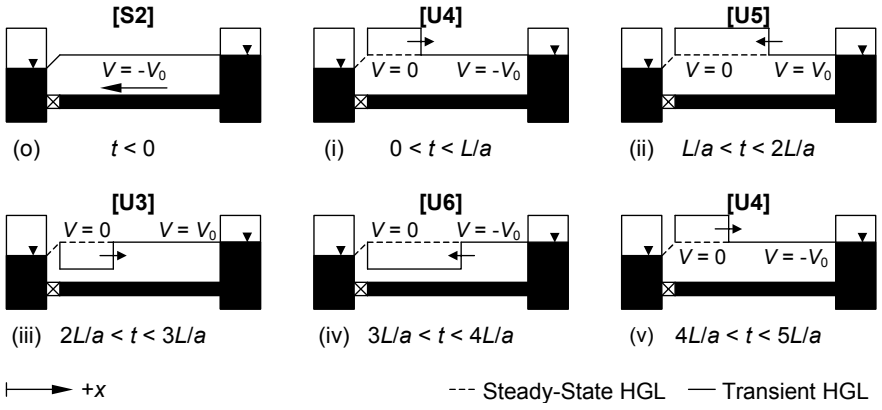

Figure 2. Transient event type E4—valve shut at $t = 0$

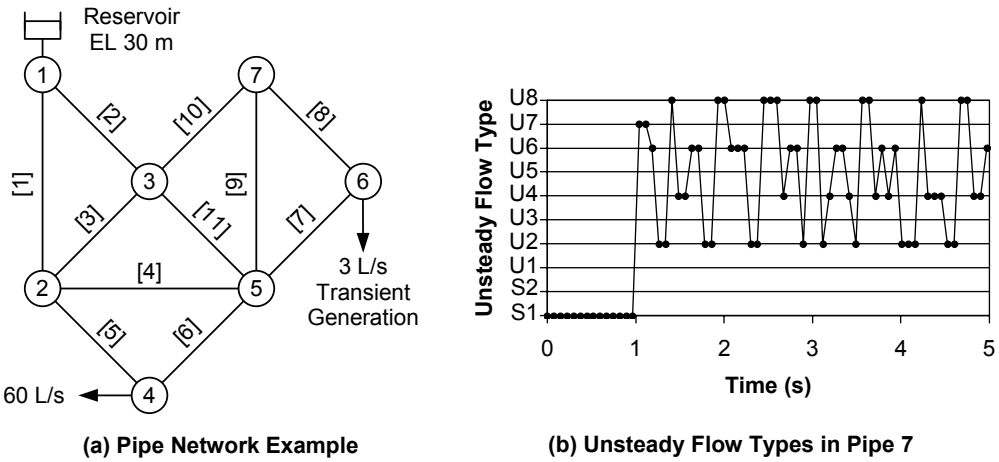

(a) Pipe Network Example **(b) Unsteady Flow Types in Pipe 7**

Figure 3. Unsteady flow types in pipe network example of Liggett and Chen (1994)

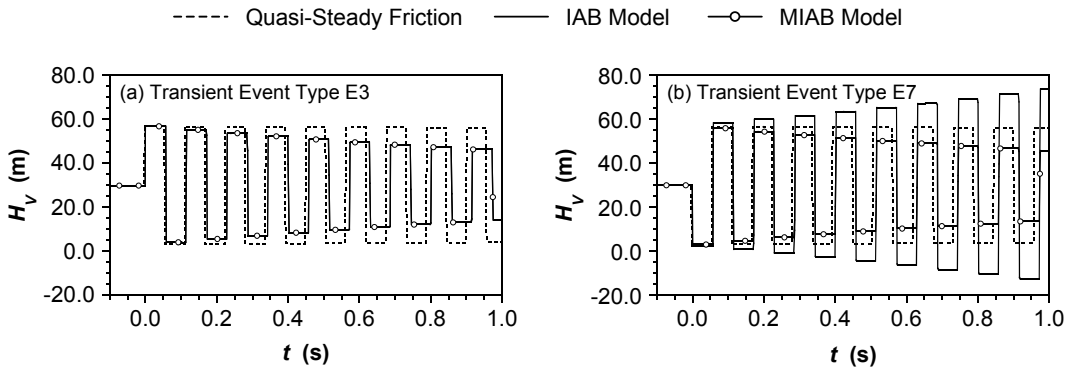

Figure 4. The IAB and MIAB models; transient event types E3 and E7

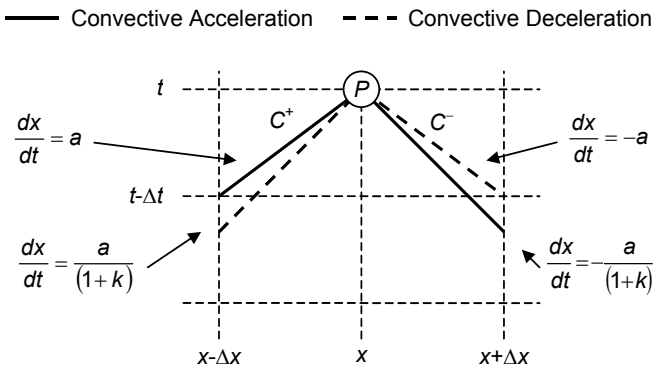

Figure 5. Variable slope characteristics of the MIAB model

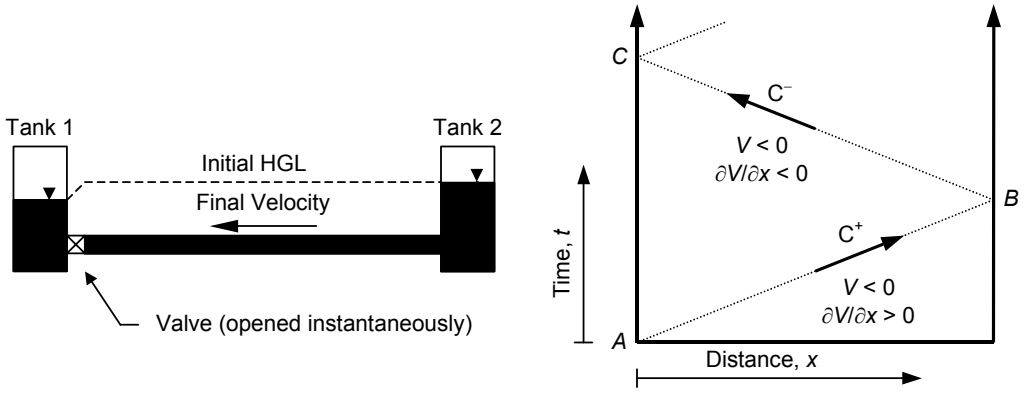

Figure 6. Example pipeline and characteristic diagram for transient event E2

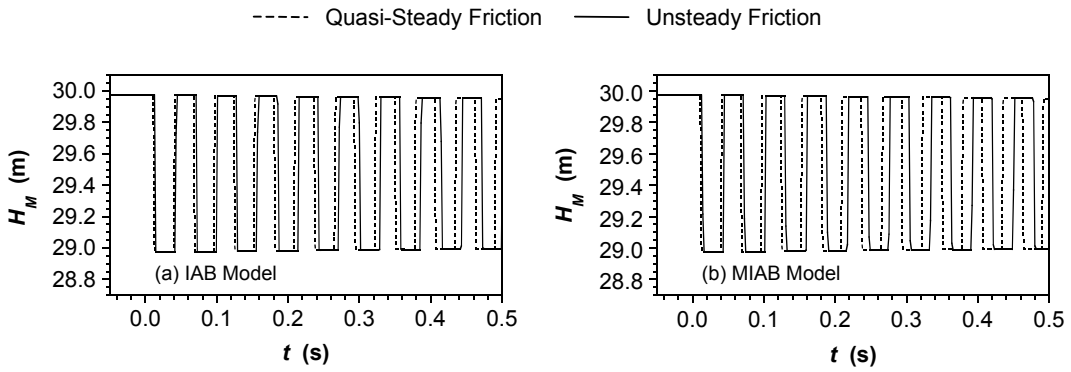

Figure 7. Lack of damping in the IAB and MIAB models; transient event type E2

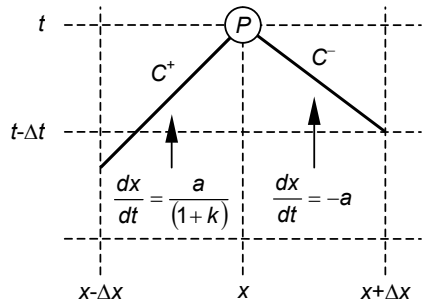

Figure 8. Characteristics for the exact solution of IAB model

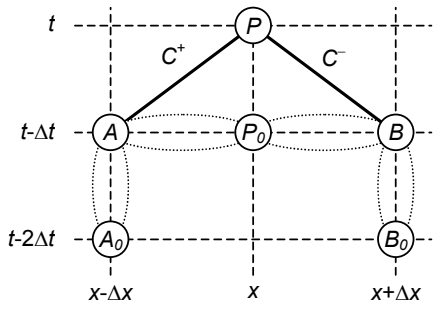

Figure 9. Derivative approximations for numerical implementation of the IAB and MIAB models

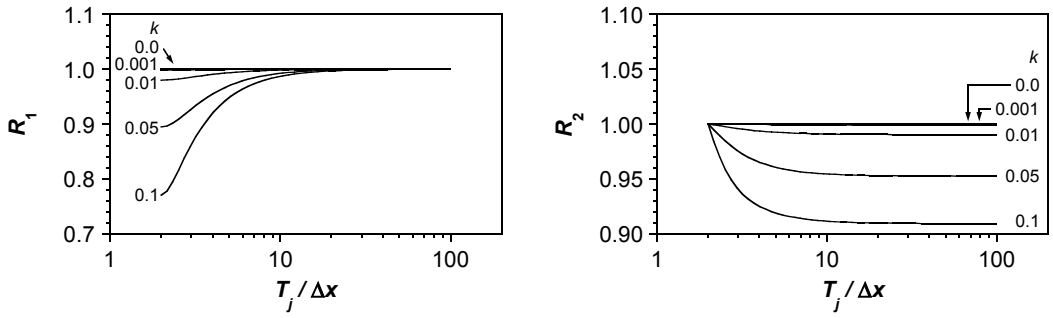

Figure 10. Variation of R_1 and R_2 with disturbance period for the numerical implementation of the IAB model

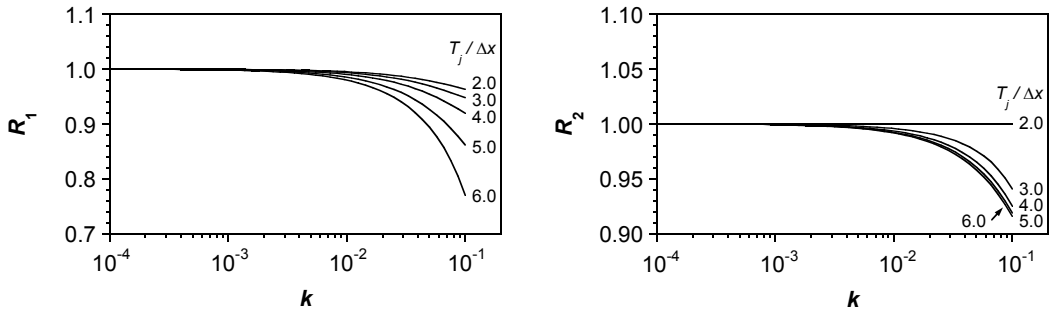

Figure 11. Variation of R_1 and R_2 with unsteady friction coefficient k for the numerical implementation of the IAB model

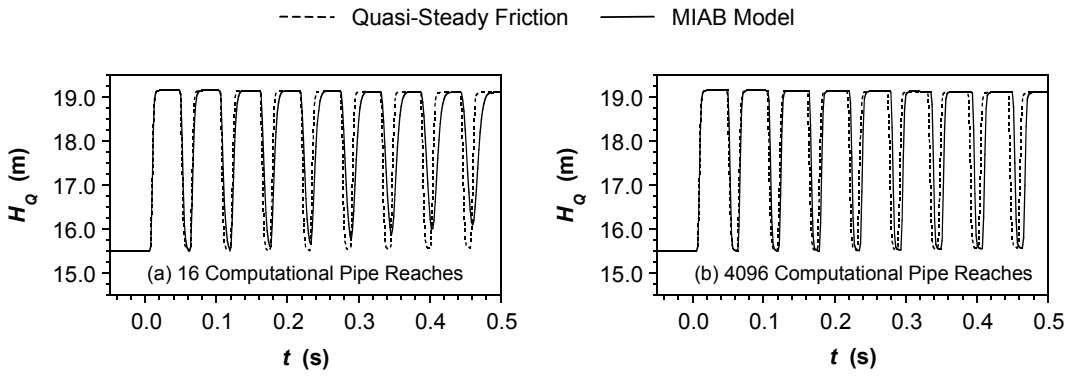

Figure 12. Numerical error using the MIAB model; transient event type E1

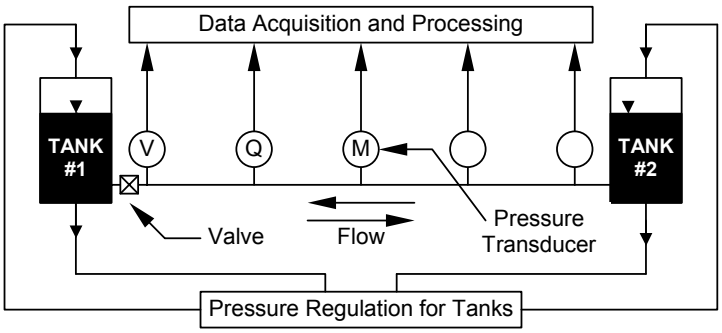

Figure 13. Experimental apparatus

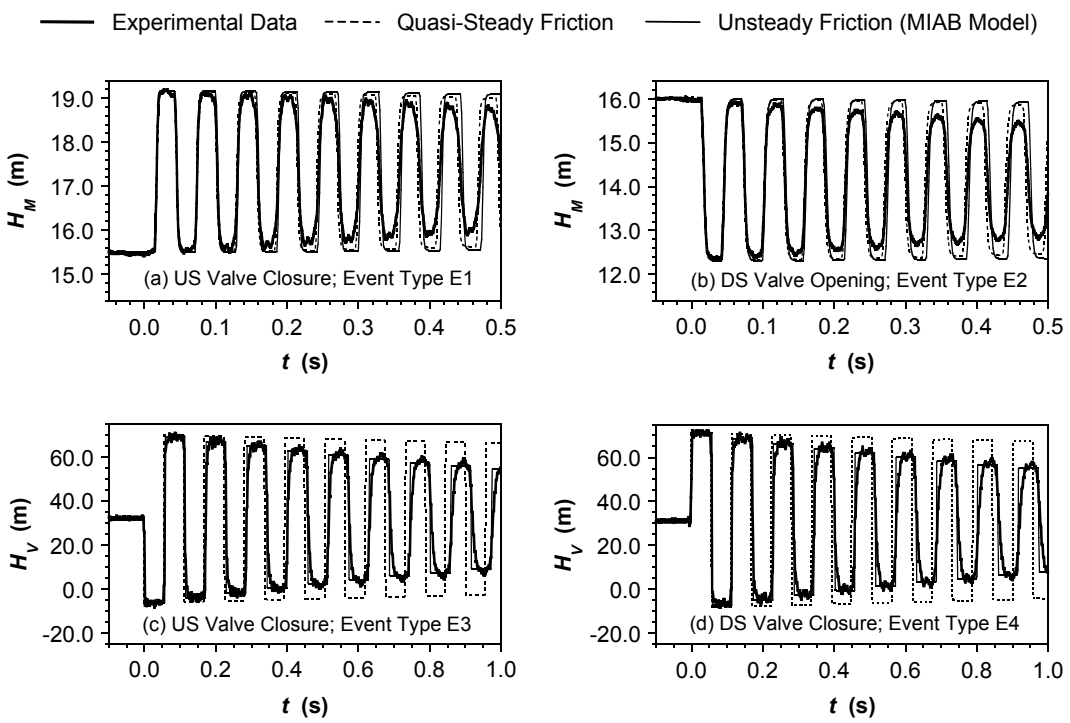

Figure 14. Experimental verification; The MIAB model using exact MOC solution

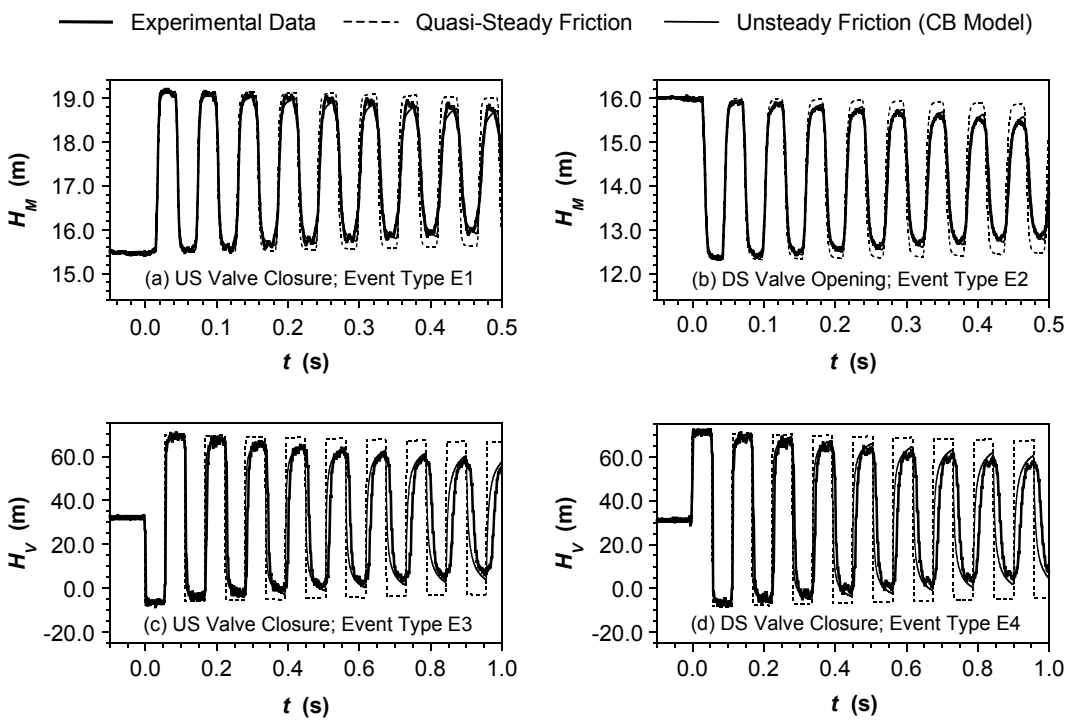

Figure 15. Experimental verification; The CB model

LIST OF TABLES

Table 1. Classification of steady and unsteady flow types

		Positive Velocity	Negative Velocity
	Steady Flow	S1	S2
Positive Wave Direction	Acceleration	U1	U2
	Deceleration	U3	U4
Negative Wave Direction	Acceleration	U5	U6
	Deceleration	U7	U8

S = Steady, U = Unsteady

Table 2. Classification of unsteady flow type sequences for each transient event type

Transient Period	Unsteady Transient Event Type							
	Opening		Closure		Opening		Closure	
	E1	E2	E3	E4*	E5	E6	E7	E8
(o)	S1	S2	S1	S2	S1	S2	S1	S2
(i)	U1	U2	U3	U4	U5	U6	U7	U8
(ii)	U5	U6	U6	U5	U1	U2	U2	U1
(iii)	U1	U2	U4	U3	U5	U6	U8	U7
(iv)	U5	U6	U5	U6	U1	U2	U1	U2
(v)	U1	U2	U3	U4	U5	U6	U7	U8

* See Figure 2

Table 3. Sign table for the IAB model

Unsteady Flow Type	J_U Component Sign		Total J_U Sign (IAB Model)	Correct J_U Sign (Golia, 1990)
	$\partial V/\partial t$	$-a\partial V/\partial x$		
U1	Positive	Positive	Positive	Positive
U2	Negative	Negative	Negative	Negative
U3	Negative	Negative	Negative	Cancellation
U4	Positive	Positive	Positive	Cancellation
U5	Positive	Negative	Cancellation	Positive
U6	Negative	Positive	Cancellation	Negative
U7	Negative	Positive	Cancellation	Cancellation
U8	Positive	Negative	Cancellation	Cancellation

Table 4. Sign table for the MIAB model

Unsteady Flow Type	J_U Component Sign		Total J_U Sign (MIAB Model)	Correct J_U Sign (Golia, 1990)
	$\partial V/\partial t$	$a\phi_4 \partial V/\partial x$		
U1	Positive	Positive	Positive	Positive
U2	Negative	Negative	Negative	Negative
U3	Negative	Positive	Cancellation	Cancellation
U4	Positive	Negative	Cancellation	Cancellation
U5	Positive	Positive	Positive	Positive
U6	Negative	Negative	Negative	Negative
U7	Negative	Positive	Cancellation	Cancellation
U8	Positive	Negative	Cancellation	Cancellation